AIMS Mathematics, 8(3): 6255–6277.
DOI: 10.3934/math.2023316
Received: 04 October 2022
Revised: 07 December 2022
Accepted: 11 December 2022
Published: 03 January 2023

http://www.aimspress.com/journal/Math

Research article

Design of neural networks for second-order velocity slip of nanofluid flow in the presence of activation energy

Kottakkaran Sooppy Nisar[1,*], Muhammad Shoaib[2,3], Muhammad Asif Zahoor Raja[4], Yasmin Tariq[5], Ayesha Rafiq[5] and Ahmed Morsy[1]

[1] Department of Mathematics, College of Arts and Science, Prince Sattam bin Abdulaziz University, Wadi Aldawaser 11991, Saudi Arabia
[2] Department of Mathematics, COMSATS University Islamabad, Attock Campus, Pakistan
[3] Yuan Ze University, AI Center, Taoyuan 320, Taiwan
[4] Future Technology Research Center, National Yunlin University of Science and Technology, 123 University Road, Section 3, Douliou, Yunlin 64002, Taiwan
[5] Department of Applied Mathematics and Statistics, Institute of Space Technology, Islamabad, Pakistan

*** Correspondence:** Email: n.sooppy@psau.edu.sa; Tel: +966563456976.

Abstract: The research groups in engineering and technological fields are becoming increasingly interested in the investigations into and utilization of artificial intelligence techniques in order to offer enhanced productivity gains and amplified human capabilities in day-to-day activities, business strategies and societal development. In the present study, the hydromagnetic second-order velocity slip nanofluid flow of a viscous material with nonlinear mixed convection over a stretching and rotating disk is numerically investigated by employing the approach of Levenberg-Marquardt back-propagated artificial neural networks. Heat transport properties are examined from the perspectives of thermal radiation, Joule heating and dissipation. The activation energy of chemical processes is also taken into account. A system of ordinary differential equations (ODEs) is created from the partial differential equations (PDEs), indicating the velocity slip nanofluid flow. To resolve the ODEs and assess the reference dataset for the intelligent network, Lobatto IIIA is deployed. The reference dataset makes it easier to compute the approximate solution of the velocity slip nanofluid flow in the MATLAB programming environment. A comparison of the results is presented with a state-of-the-art Lobatto IIIA analysis method in terms of absolute error, regression studies, error histogram analysis, mu, gradients and mean square error, which validate the performance of the proposed neural networks. Further, the impacts of thermal, axial, radial and tangential velocities on the stretching parameter, magnetic variable, Eckert number, thermal Biot numbers and second-order slip parameters are also examined in this article. With an increase in the stretching parameter's values, the speed increases. In contrast, the temperature profile drops as the magnetic variable's value increases. The technique's

worthiness and effectiveness are confirmed by the absolute error range of 10^{-7} to 10^{-4}. The proposed system is stable, convergent and precise according to the performance validation up to E^{-10}. The outcomes demonstrate that artificial neural networks are capable of highly accurate predictions and optimizations.

Keywords: velocity slip; artificial neural network; Levenberg-Marquardt; Lobatto IIIA; activation energy
Mathematics Subject Classification: 68T20, 70E99, 35-XX

1. Introduction

Artificial neural networks (ANNs) are a significant technique for artificial intelligence. ANNs have developed applications in a wide range of fields owing to their capacity to refabricate and model nonlinear phenomena. System identification, sequence recognition, process control, sensor data analysis, natural resource management, quantum chemistry, data mining, pattern recognition, medical diagnosis, finance, visualization, machine translation, e-mail spam filtering and social network filtering are just a few examples of its applications based on the input that flows via a network during the learning process, either externally or internally, ANNs are evolutionarily versatile under a variety of conditions. The back propagation helps to reliable back propagation stochastic numerical technique. Backpropagation is a supervised learning method that applies the gradient descent approach to lower the gradient of the error curve and thereby minimize error. Paul Werbos devised the backpropagation method in 1974, which Rumelhart and Parker rediscovered. In feed-forward multilayer neural networks, the backpropagation algorithm is commonly used as a learning method. The Levenberg-Marquardt (LM) backpropagation technique for ANNs is a ground-breaking convergent stability methodology that gives numerical solutions to a large extent of fluid flow issues. Numerous researchers have recently experimented with Newtonian and non-Newtonian fluid systems by using an Levenberg-Marquardt back-propagated ANN (LBM-BN). Ly et al. [1] provided a metaheuristic analysis for the parameters and construction of LBM-BN to forecast the shear capacity of foamed concrete accurately and quickly. Zhao et al. [2] used the LBM-BN method to estimate the defection of reinforced concrete beams. Nguyen et al. [3] used ANN-based LM to improve the reliability of robot placement. The ANN approach was adopted by Ali et al. [4] to estimate the expulsion over a sharp-crested weir, and the training technique is based on LM. Ye and Kim [5] used an LBM-BN in China to evaluate electricity usage in a building. Bharati et al. [6] created a neuro-fuzzy system framework and self-organizing maps for superconductor prediction.

Nanofluids are usually utilized as coolants in heat transfer devices such as heat exchangers, electronic cooling systems and radiators because of their improved thermal properties. Nanofluids have unique characteristics that could make them fruitful in a variety of heat transfer applications, including pharmaceutical practices, microelectronics and hybrid-powered engines, as well as in engine cooling, heat exchangers, domestic refrigerators, grinding, chillers and boiler flue gas temperature reduction. Numerous studies based on the nanofluid concept have been published in the previous few decades. Choi and Eastman [7] proposed nanoparticle diffusion in a base fluid for engineering disciplines for the first time two decades ago. In an analysis by Uddin et al. [8], in the presence of a stretching and contracting sheet, steady two-dimensional laminar mixed convective boundary slip nanofluid flow arises in a permeable Darcian medium. A Din et al. [9] investigation found that the temperature dispersion, productivity and temperature of the fin's tip are significantly influenced by thermal and

thermo-geometric aspects. According to their analysis, the fading exponential fin is more efficient than the expanding exponential fin, and this offers important benefits for mechanical engineering. The results on a magnetohydrodynamics (MHD) nanofluid in a circular permeable material, as presented by Jalili et al. [10], demonstrates that the convection mechanism weakens with an increase in the volume fraction of solid nanoparticles. A stronger and more unified core vortex will result from a substantial rise in the Rayleigh number. Additionally, a favorable Nuave occurs when a magnetic force is applied horizontally. A ferrofluid over a shrinking sheet with effective thermal conductivity was another subject of study by Jalili et al [11]. The results indicate that the magnetic and boundary parameters have a similar effect on velocity as the micro-rotation parameter. By examining natural convection in a cavity equipped with a nanofluid, Geridonmez reported in [12] that the fluid velocity and heat transmission are boosted in the presence of nanoparticles, and that convective heat transfer is decreased in a rectangular cavity. The squeezing nanofluid flow that was developed by the authors of [13,14] investigated the Casson-type hybrid nanofluid with slip and sinusoidal heat conditions. Tawade et al. [15] observed increments in the temperature profile for increasing values of the Brownian motion parameter, and that the energy distribution increases with increment in the value of the thermophoresis parameter. Hamid et al. [16] investigated the fractional-order unsteady natural convective radiating flow of a nanofluid; they observed that the velocity field decreases with enhancing magnetic field effects. A heat and mass transmission study of radiative and chemical reactive effects on an MHD nanofluid over an infinite moving vertical plate was performed by Arulmozh et al. [17]. The behavior of an ionized nano-liquid motion with reference to heat transmission between two parallel discs was studied by Khan et al. [18]. Tuz Zohra et al. [19] explored the MHD bio-nano convective slip stream with Stefan blowing phenomena across a spinning disc, demonstrating that, compared to blowing, suction offers a better medium for enhancing the amount of heat, mass and microbial transmission. Various studies pertaining to nanofluids can be found in [20–23].

The activation energy (AE) in a fluid stream is significant in a broad range of industrial applications. Arrhenius proposed the concept of activation energy in 1889. It is the absolute basic minimum of energy required for the organisms to transform the reaction mixture into products. Oil emulsions, geothermal energy, fluid mechanics and chemical engineering all benefit from this phenomenon. Given a Carreau nanofluid with magnetic influence, Irfan et al. [24] applied mass flux theory and Arrhenius activation energy. Waqas et al. [25] proposed a bio-convection flow of a tangent hyperbolic nanofluid over a Riga plate with activation energy, demonstrating that increasing the chances of mixed convection parameters increases the velocity of the tangent hyperbolic fluid. Bhatti and Michaelides [26] also used activation energy to transmit a thermo-bioconvection nanofluid across a Riga plate. The nanofluid and bacteria existing in the base fluid were filled into the Riga plate. The study of modulated heat plus mass fluxes in 3D Eyring-Powell nanofluid nonlinear thermal radiation was done by Muhammad et al. [27]. For preventing boundary-layer separation and reducing submarine friction and pressure drag, a Riga plate has been used. In the presence of electromagnetic fields and gyrotactic microorganisms, slip effects on an MHD nanofluid were explored by Habib et al. [28], who used a mathematical approach. The MHD peristaltic transport of a Sutterby nanofluid with mixed convection and a Hall current was described by Hayat et al. [29]. In contrast to higher activation energies and radiation factors, concentration was seen to increase. Entropy continues to decrease in response to greater diffusion parameters.

In real-life situations, many complex problems demand an ANN due to their complex structure. Due to their extensive applicability in a wide range of domains, analytical and numerical actions that address computational fluid dynamic problems with a deterministic computing model are garnering increasing interest from technical groups, specifically, mathematicians and physicists. When compared

to traditional numerical techniques, artificial intelligence algorithms based on stochastic numerical computing have produced accurate and validated results, inspiring authors to work in this paradigm. Researchers in ANNs have recently accomplished some valuable work, like entropy-generated systems [30], porous fins [31], COVID-19 [32], hydromagnetic Williamson fluid flow [33], carbon nanotubes [34], Emden-Fowler equation [35], second-order singular functional differential models [36], Darcy-Forchheimer models [37], dissipative fluid flow systems [38], mosquito dispersal models [39] and many others [40–43].

The authors' main goal of this paper is to exploit the strength of artificial back-propagated neural networks with an LBM-BN algorithm that augment the computing power and level of accuracy of the solver to scrutinize the hydromagnetic velocity slip nanofluid flow (VSN) of a viscous material with nonlinear mixed convection over a stretching and rotating disc. No one has used this technique for the proposed problem. It is a novel approach to solve the problem of intelligent computing technique-based supervised learning for VSN model dynamics by using a modern stochastic solution approach based on the artificial intelligence algorithm. Artificial intelligence-based stochastic solution approaches are a more effective and practical substitute for the implementation of numerous linear and nonlinear mathematical frameworks. These problem-solving methods were developed by using a contemporary computing paradigm to address a system of extremely nonlinear ordinary differential equations (ODEs) that describe the mathematical representations of such fluid problems. The main objectives of this research are as follows:

(i). Represent the mathematical modeling for hydromagnetic VSN.
(ii). Explain the solution for designed hydromagnetic VSN via testing, validation and training processes.
(iii). Examine the reference data samples arbitrarily preferred for testing, training and validation and analyze the approximated solutions of the proposed LBM-BN in comparison with the reference results.
(iv). Generate datasets through the use of LM, and in training/validation/testing processes, as a target for identifying the approximated solution of the proposed LBM-BN.
(v). The suggested technique efficiently examines the dynamics of the problem for many scenarios based on the variation of pertinent parameters to depict velocity, concentration and temperature profiles.
(vi). The LBM-BN validity and verification are based on a thorough examination of accuracy assessments, histograms and regression analysis conducted for the VSN, which are given graphically and numerically in sufficient detail.
(vii). Examine the various scenarios of the VSN by varying the stretching parameter, magnetic variable, Eckert number, thermal Biot numbers and second-order slip parameters.

The proposed mathematical model is illustrated in Section II. Section III describes the methodology of the designed LBM-BNs with the interpretation of the result. Section IV discusses the effects of several physical parameters on axial $f(\xi)$, radial $f'(\xi)$, thermal $\theta(\xi)$, and tangential velocities $g(\xi)$. The current study's conclusion is drawn in Section V.

2. Problem model

Nonlinear mixed convection hydromagnetic slip flow for nanofluid flow is considered. The slip velocity is of second order. The considered fluid is incompressible, electrically conductive and flowing along a stretching and rotating surface. The disk is located at z = 0 and rotating with a frequency Ω about the z axis. At $z > 0$, the heat transfer is taken out matter to thermal radiation, Joule heating,

Brownian motion and thermophoresis diffusion are also incorporated in the fluid flow system. Figure 1 is a physical illustration of the model.

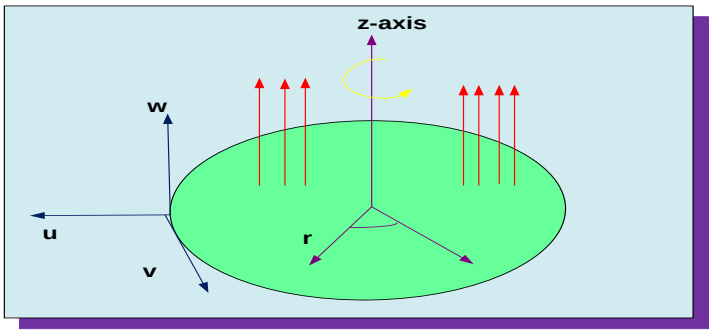

Figure 1. Problem model.

The governing flow model is given in [44–47]. The stimulated magnetic field is ignored because of small values of the following:

$$\frac{\partial w}{\partial z}+\frac{u}{r}+\frac{\partial u}{\partial r}=0, \tag{1}$$

$$\frac{\partial u}{\partial z}w-\frac{v^2}{r}+\frac{\partial u}{\partial r}u$$

$$\frac{\partial^2 u}{\partial z^2}\nu_f-\frac{\sigma_f}{\rho_f}B_0^2u+g\{\beta_1(T-T_\infty)+\beta_2(T-T_\infty)^2+\beta_3(C-C_\infty)+\beta_4(C-C\infty)^4\}, \tag{2}$$

$$\frac{\partial v}{\partial z}w+\frac{\partial v}{\partial r}u+\frac{uv}{r}=\frac{\partial^2 v}{\partial z^2}\nu_f-\frac{\sigma_f}{\rho_f}B_0^2v, \tag{3}$$

$$\left(\frac{\partial T}{\partial z}w+\frac{\partial T}{\partial r}u\right)=\frac{\partial^2 T}{\partial z^2}\frac{\kappa_f}{(\rho c_p)_f}+\frac{(\rho c_p)_p}{(\rho c_p)_f}\left\{\left(\frac{\partial T}{\partial z}\right)^2\frac{D_T}{T_\infty}+\left(\frac{\partial C}{\partial z}\cdot\frac{\partial T}{\partial z}\right)D_B\right\}$$

$$+\left\{\left(\frac{\partial v}{\partial z}\right)^2+\left(\frac{\partial u}{\partial z}\right)^2\right\}\frac{\mu_f}{(\rho c_p)_f}+\frac{\sigma_f B_0^2}{(\rho c_p)_f}(u^2+v^2)+\frac{\partial^2 T}{\partial z^2}\frac{16\sigma\ T_\infty^3}{3\kappa\ (\rho c_p)_f}, \tag{4}$$

$$\frac{\partial C}{\partial z}w+\frac{\partial C}{\partial r}u=\frac{\partial^2 C}{\partial z^2}D_B+\frac{\partial^2 T}{\partial z^2}\frac{D_T}{T_\infty}-\kappa_r^2(C-C_\infty)\left(\frac{T}{T_\infty}\right)^n exp\left(\frac{-E_\alpha}{\kappa T}\right), \tag{5}$$

$$u=a_1r+\frac{\partial u}{\partial z}\lambda_1+\frac{\partial^2 u}{\partial z^2}\lambda_2, v=\Omega r+\frac{\partial v}{\partial z}\lambda_3+\frac{\partial^2 v}{\partial z^2}\lambda_4, w=0,$$

$$\frac{-\partial T}{\partial z}\kappa_f=(T_w-T)h_1, -\frac{\partial C}{\partial z}D_B=(C_w-C)h_2 atz=0, \tag{6}$$

$$u\to 0, v\to 0, T\to T\infty, C\to C_\infty whenz\to\infty.$$

Here, from [46],

$$u=r\Omega f', v=r\Omega g, w=-2h\Omega f, \phi=\frac{C-C_\infty}{C_w-C_\infty}, \theta=\frac{T-T_\infty}{T_w-T_\infty}, \zeta=\frac{z}{h}. \tag{7}$$

The dimensionless equations are as follows:

$$f'''+\Re(2ff''-f'^2+g^2-Mf')+\lambda\theta(1+\beta_t\theta)+\lambda N\quad\phi(1+\beta_c\phi)=0, \tag{8}$$

$$g''+\Re(2fg'-2f'g-Mg)=0, \tag{9}$$

$$\frac{1}{Pr}(R+1)\theta''+2Ref\theta'+Nt\theta'^2+Nb\theta'\phi'+MEc(f'^2+g^2)+Ec, \tag{10}$$

$$\frac{1}{Sc}\phi+\mathrm{f}\phi'+\{1\}\mathrm{over}\{\mathrm{Sc}\}\mathrm{left}(\{\mathrm{Nt}\}\mathrm{over}\{\mathrm{Nb}\}\mathrm{right})\theta - \kappa_1\phi(1+\alpha_1\theta)^n exp\left(\frac{-E_1}{1+\alpha_1\theta}\right) = 0, \tag{11}$$

$$f'(0) = A_1 + L_1 f''(0)+\mathrm{L}_2\mathrm{f}'\mathrm{left}(0\mathrm{right}), f\mathrm{left}(0\mathrm{right}) = 0,$$

$$g\mathrm{left}(0\mathrm{right}) = 1 + \{L\}\mathrm{rsub}\{3\}g'\mathrm{left}(0\mathrm{right}) + \{L\}\mathrm{rsub}\{4\}g''\mathrm{left}(0\mathrm{right}),$$

$$\theta'(0) = -B_1\big(1-\theta(0)\big), \phi'(0) = -B_2\big(1-\phi(0)\big), atz = 0, \tag{12}$$

$$f'(\infty)\to 0, g(\infty)\to 0, \theta(\infty)\to 0, \phi(\infty)\to 0.$$

Here,

$$\Re = \frac{r^2\Omega}{\nu_f}, M = \frac{\sigma_f B_0^2}{\rho_f a}, \lambda = \frac{g\beta_1(T_w-T_\infty)}{r\Omega^2}, N = \frac{\beta_3(C_w-C_\infty)}{\beta_1(T_w-T_\infty)}, Pr = \frac{(\rho c_p)_f \nu_f}{\kappa_f},$$

$$R = \frac{16\sigma\ \ T_\infty^3}{3\kappa_f\kappa}, Nt = \frac{\tau D_T(T_w-T_\infty)}{T_\infty\nu_f}, Ec = \frac{(r\Omega)^2}{c_p(T_w-T_\infty)}, Nb = \frac{\tau D_B(C_w-C_\infty)}{\nu_f}, Sc = \frac{\nu_f}{D_B},$$

$$\kappa_1 = \frac{\kappa_r^2}{\Omega}, \alpha_1 = \frac{(T_w-T_\infty)}{T_\infty}, \beta_t = \frac{\beta_2(T_w-T_\infty)}{\beta_1}, \beta_c = \frac{\beta_4(C_w-C_\infty)}{\beta_3}, E_1 = \frac{E_a}{\kappa T_\infty}, A_1 = \frac{a_1}{\Omega},$$

$$L_1 = \frac{\lambda_1}{h}, L_2 = \frac{\lambda_2}{h^2}, L_3 = \frac{\lambda_3}{h}, L_4 = \frac{\lambda_4}{h^2}, B_1 = \frac{h_1 h_2}{\kappa_f}, B_2 = \frac{h_2 h}{D_B}, \kappa = 8.61\times 10^{-5}\ eV/K.$$

3. Solution methodology

The novel concept of the proposed LBM-BN-based method is applied to examine the steady 3D incompressible hydromagnetic VSN flow for a rotating disc surface with nonlinear mixed convection. Nonlinear PDEs are altered into ODEs through appropriate transformations, and the computational results can be calculated by utilizing the Lobatto IIIA formula in the bvp4c technique in MATLAB software. For boundary-value problems, the Lobatto IIIA approach has been studied to test the stability of attributes. The Lobatto IIIA method is used by many researchers in different fields [48–51]. This technique is applied for the solution of ODEs and generates a dataset for the LBM-BN. The datasets are attained from Lobatto IIIA based on the variation of influential parameters. Later on, a solution can be approximated through a training, testing and validation procedure in MATLAB by using the nftool module, and a comparison is made between the standard results and those of the LBM-BN. The designed neural network weights are connected with nodes and optimized via hidden layers and activation functions. If the weights are not optimized through a forward pass, then the backward pass is taken into account to tune the values of weights, which provides the best solution for the governing mathematical systems. The procedure for the ANNs is provided in [52,53]. This dataset can be used to assist in the calculation of the approximated solution of the VSN problem in MATLAB. Figure 2 illustrates the ANN for the VSN. Figure 3 illustrates the flowchart for the given problem. Regarding the influence of different parameters of the VSN, the graphs are presented for axial $f(\xi)$, radial $f'(\xi)$, thermal $\theta(\xi)$, and tangential velocity $g(\xi)$ profiles. Also, Table 1 shows all of the scenarios and cases for variants of the VSN. Table 2 reflects the outcomes of the LBM-BN for all scenarios of the VSN. Table 2 contains the epochs, mean square error (MSE) values, performances, mu parameters, gradients and times for all scenarios related to the VSN. For validation of the performance of the LBM-BN, error histogram (EH) regression analysis was performed and the transition state (TS) and MSE results are analyzed.

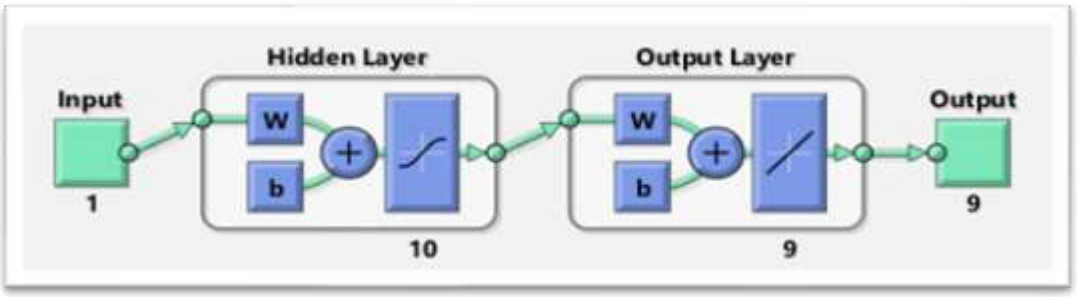

Figure 2. Neural network of VSN.

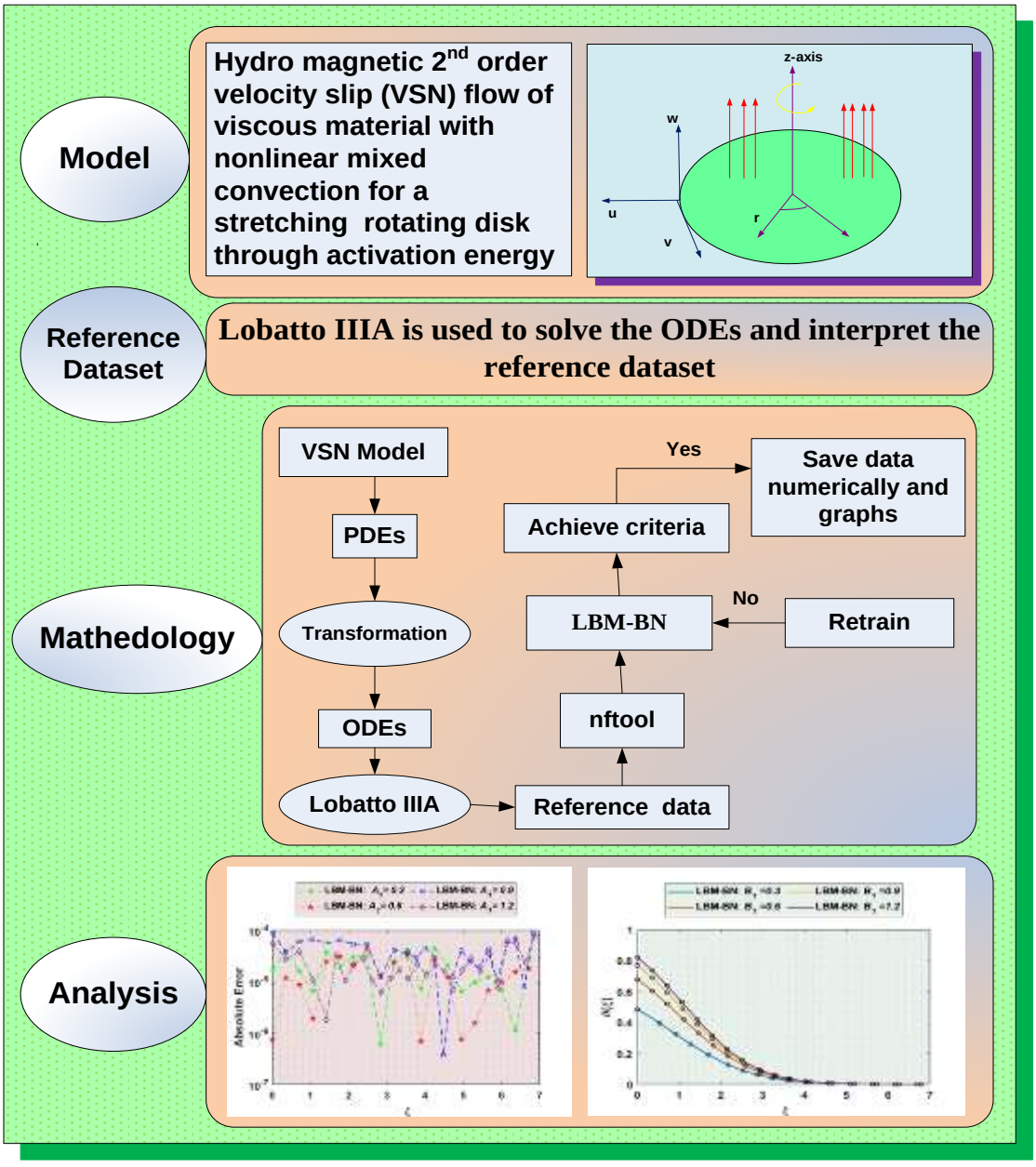

Figure 3. Flowchart.

4. Results and discussion

The effects of the VSN model were resolved by using an ANN with back-propagated LM. The reference dataset was generated by applying the Lobatto IIIA procedure using MATLAB software. The numerical solution achieved for the allocation of axial $f(\xi)$, radial $f'(\xi)$, thermal $\theta(\xi)$, and tangential velocity $g(\xi)$ profiles has been studied and explained through diagrams. All six different scenarios of each have four different cases that are listed in Table 1. The input ranged between 0 and 7, with a step size of 0.07 for each case of the proposed LBM-BN for the VSN model. After the dataset was generated, the 'nftool' command was employed to evaluate the solution for the VSN. The solutions of the LBM-BN for all scenarios of Case IV, in the form of the MSE, curve fitness plot, error histogram, regression and training state, are demonstrated in Figures 4–8. Figures 4–8 show the outcomes of the stretching parameter (A_1), magnetic variable $(M$, Eckert number (Ec), thermal Biot numbers (B_1), and second-order slip parameters (L_2, L_4) for the VSN model. Additionally, convergence through MSE curves for training and testing, as well as the gradient, best performance index, time taken, mu and epochs are presented in Table 2 for each scenario of all four cases.

Figure 4 shows the training, validation and testing MSE curves for Case IV for all six scenarios of the VSN. Figure 4(a) shows the MSE curves for Scenario 1 of Case IV. The MSE curves for the best validation performance were attained at 2.97E-10 with 145 epochs in 9 s. Figure 4(b) shows the MSE curves for Scenario 2 of Case IV. The MSE curves for the best validation performance were attained at 3.42E-10 with 84 epochs in 1 s. Figure 4(c) shows the MSE curves for Scenario 3 of Case IV. The MSE curves for the best validation performance were attained at 6.22E-11 with 58 epochs in 0 s. Figure 4(d) shows the MSE curves for Scenario 4 of Case IV. The MSE curves for the best validation performance were attained at 2.25E-10 with 148 epochs in 0 s. Figure 4(e) shows the MSE curves for Scenario 5 of Case IV. The MSE curves for the best validation performance were attained at 1.20E-09 with 103 epochs in 0 s. Figure 4(f) shows the MSE curves for Scenario 6 of Case IV. The MSE curves for the best validation performance were attained at 2.54E-09 with 193 epochs in 1 s.

Figure 5 illustrates the TS for Case IV for all six scenarios, which was obtained by using the LBM-BN. The impacts of the axial $f(\xi)$, radial $f'(\xi)$, temperature $\theta(\xi)$, and tangential velocities $g(\xi)$ on the stretching parameter (A_1), magnetic variable $(M$, Eckert number (Ec), thermal Biot number (B_1), and second-order slip parameters (L_2, L_4) were investigated. The gradient had values of 9.93E-08, 9.95E-08, 9.66E-08, 9.90E-08, 9.67E-08 and 9.71E-08, where the values of the mu parameter were 1.00E-08, 1.00E-09, 1.00E-10, 1.00E-09, 1.00E-09 and 1.00E-09 for the LBM-BN, as shown in the depicted plots. The enhanced networks training and test the enhanced convergence of the results can be obtained for the smallest values of gradient, and Mu provide the best convenience.

Figures 6(a–f) and 7(a–f) represent the fitness curves and EHs for Case IV in terms of A_1, M, L_2, L_4, B_1 and Ec, as obtained by using the LBM-BN for the VSN model. The scrutiny of the EHs reveals that the maximum values depicting the errors were found to be very close to zero, which validates the worth of the solver.

Figure 8(a–f) reflects the graphical illustration of the regression analysis for Case IV for all scenarios of the LBM-BN VSN. The regression plots show that the solver gave the most optimal solution corresponding to the scenarios in terms of A_1, M, L_2, L_4, B_1 and $Ecforf(\xi), f'(\xi), g(\xi), \wedge \theta(\xi)$, as associated with the presented fluid flow system.

Figure 9 demonstrates the behavior of all physical quantities A_1, M, L_2, L_4, B_1 and Ec for $f(\xi)$, $f'(\xi), g(\xi), \wedge \theta(\xi)$. From Figure 9(a,b) it can be perceived that, for a higher value of A_1, the flow increases in the radial and axial velocity directions. Substantially, for a larger A_1, the stretching rate increases and creates more disturbance in the liquid. Thus, the velocity increases. Figure 9(c,d) shows

the effect of L_2 for $f(\xi),\wedge f'(\xi)$. Clearly, we examined that the velocity components $f(\xi),\wedge f'(\xi)$decline due to an enrichment in L_2.

Figure 9(e) depicts the impact of the tangential velocity $g(\xi)$ due to the second-order slip parameter L_4. It can be seen that the tangential velocity declines with the increase of second order slip parameter.

The effects of reducing the influence of the tangential velocity and its relationship with larger values of M are depicted in Figure 9(f). Physically, for larger values of *M*, the Lorentz force increases, which is a force that is resistant to the motion of producing material elements. Hence, the velocity decreases. Figure 9(g) displays the effect of Ec on temperature. The parameter Ec was used to calculate the effect of self-heating on the dissipation properties of a liquid. At extreme flow rates, the thermal field in a fluidic framework is swamped by the temperature gradients appearing in the framework. Also, the effects of dissipation caused by the internal friction temperature are enhanced with the increase of Ec. Figure 9(h) was sketched to discuss the performance of B_1 on temperature function. We can see that $\theta(\xi)$ increases with increment in the value of B_1.

Figure 10 shows the graphical representation of absolute error (AE) with the variation of $f(\xi)$, $f'(\xi)$, $g(\xi)$ and $\theta(\xi)$, which validates the performance of the proposed technique. In Figure 10(a), the AE lies between 10^{-4} and 10^{-7} with the increment in A_1 for $f(\xi)$, whereas, in Figure 10(b), the AE ranges between 10^{-4} and 10^{-6} with the increase in A_1 for $f'(\xi)$. Figure 10(c, d) illustrates the AE of $L_2$for $f(\xi)$ and $f'(\xi)$ in the range of 10^{-4} to 10^{-7}. Figure 10(e, f) depicts the AE of L_4 and M for the tangential velocity $g(\xi)$in the range of 10^{-4} to 10^{-7} and 10^{-4} to 10^{-6}, respectively. Figure 10(g, h) exhibits the AE in the range of 10^{-4} to 10^{-7} for both *Ec* and B_1 for the temperature function $\theta(\xi)$.

Table 1. All scenarios and cases for physical quantities of the VSN.

Scenario	Physical Quantities	Profile	Cases			
			Case 1	Case 2	Case 3	Case 4
1	A_1	$f(\chi)$	0.3	0.6	0.9	1.2
		$f'(\chi)$	0.3	0.6	0.9	1.2
2	L_2	$f(\chi)$	-0.3	-0.6	-0.9	-1.0
		$f'(\chi)$	-0.3	-0.6	-0.9	-1.0
3	L_4	$g(\chi)$	-0.15	-0.3	-0.45	-0.6
4	M	$g(\chi)$	1.0	2.0	3.0	4.0
5	Ec	$\theta(\chi)$	0.2	0.4	0.6	0.8
6	B_1	$\theta(\chi)$	0.3	0.6	0.9	1.2

Table 2. Outcomes of LBM-BN for all scenarios of the VSN.

Scenario	Case	MSE			Performance	Mu parameter	Gradient	Epochs	Time
		Training	Validation	Testing					
S-I	I	3.83E-10	5.45E-10	4.93E-10	3.83E-10	1.00E-08	9.93E-09	127	2 s
	II	2.81E-10	2.29E-10	3.33E-10	2.81E-10	1.00E-09	9.78E-07	104	1 s
	III	7.39E-10	8.33E-10	8.29E-10	7.40E-09	1.00E-08	9.84E-08	161	2 s
	IV	2.32E-10	2.97E-10	2.44E-10	1.10E-08	1.00E-08	9.93E-08	107	9 s
S-II	I	3.40E-10	4.88E-10	3.69E-10	3.41E-10	1.00E-09	9.84E-08	126	0 s
	II	3.03E-11	3.14E-11	4.44E-11	3.04E-11	1.00E-10	9.79E-08	63	1 s
	III	2.18E-11	2.67E-11	1.94E-11	2.19E-11	1.00E-10	9.93E-08	65	1 s
	IV	2.84E-10	3.42E-10	3.38E-10	2.84E-10	1.00E-09	9.95E-07	84	1 s
S-III	I	3.14E-10	3.96E-10	3.16E-10	3.15E-10	1.00E-09	9.76E-09	133	1 s
	II	3.25E-11	3.74E-11	6.04E-11	3.25E-11	1.00E-10	9.85E-08	76	0 s
	III	4.08E-11	4.75E-11	6.16E-11	4.08E-11	1.00E-10	9.75E-07	56	0 s
	IV	5.57E-11	6.22E-11	7.19E-11	5.57E-11	1.00E-10	9.66E-08	58	0 s
S-IV	I	8.82E-10	9.32E-10	1.78E-09	8.83E-10	1.00E-09	9.97E-08	122	1 s
	II	3.65E-09	4.73E-09	3.86E-09	3.65E-09	1.00E-09	9.86E-08	50	0 s
	III	1.82E-09	4.45E-09	3.02E-09	1.82E-09	1.00E-09	9.76E-08	83	0 s
	IV	1.69E-10	2.25E-10	1.41E-10	1.70E-10	1.00E-09	9.90E-08	148	0 s
S-V	I	4.01E-10	4.19E-10	4.86E-10	4.01E-10	1.00E-09	9.99E-09	151	1 s
	II	5.36E-10	8.74E-10	6.63E-10	5.36E-10	1.00E-09	9.81E-08	126	0 s
	III	7.90E-10	7.35E-10	7.61E-10	7.91E-10	1.00E-09	9.54E-07	107	0 s
	IV	9.13E-10	1.20E-09	9.52E-10	9.14E-10	1.00E-09	9.67E-08	103	0 s
S-VI	I	1.76E-09	1.73E-09	1.66E-09	1.76E-09	1.00E-09	9.92E-07	76	0 s
	II	1.08E-09	1.18E-09	1.26E-09	1.08E-09	1.00E-09	9.86E-08	96	0 s
	III	2.03E-09	2.28E-09	2.13E-09	2.04E-09	1.00E-09	9.93E-09	68	0 s
	IV	2.20E-09	2.54E-09	2.36E-09	2.21E-09	1.00E-09	9.71E-08	193	1 s

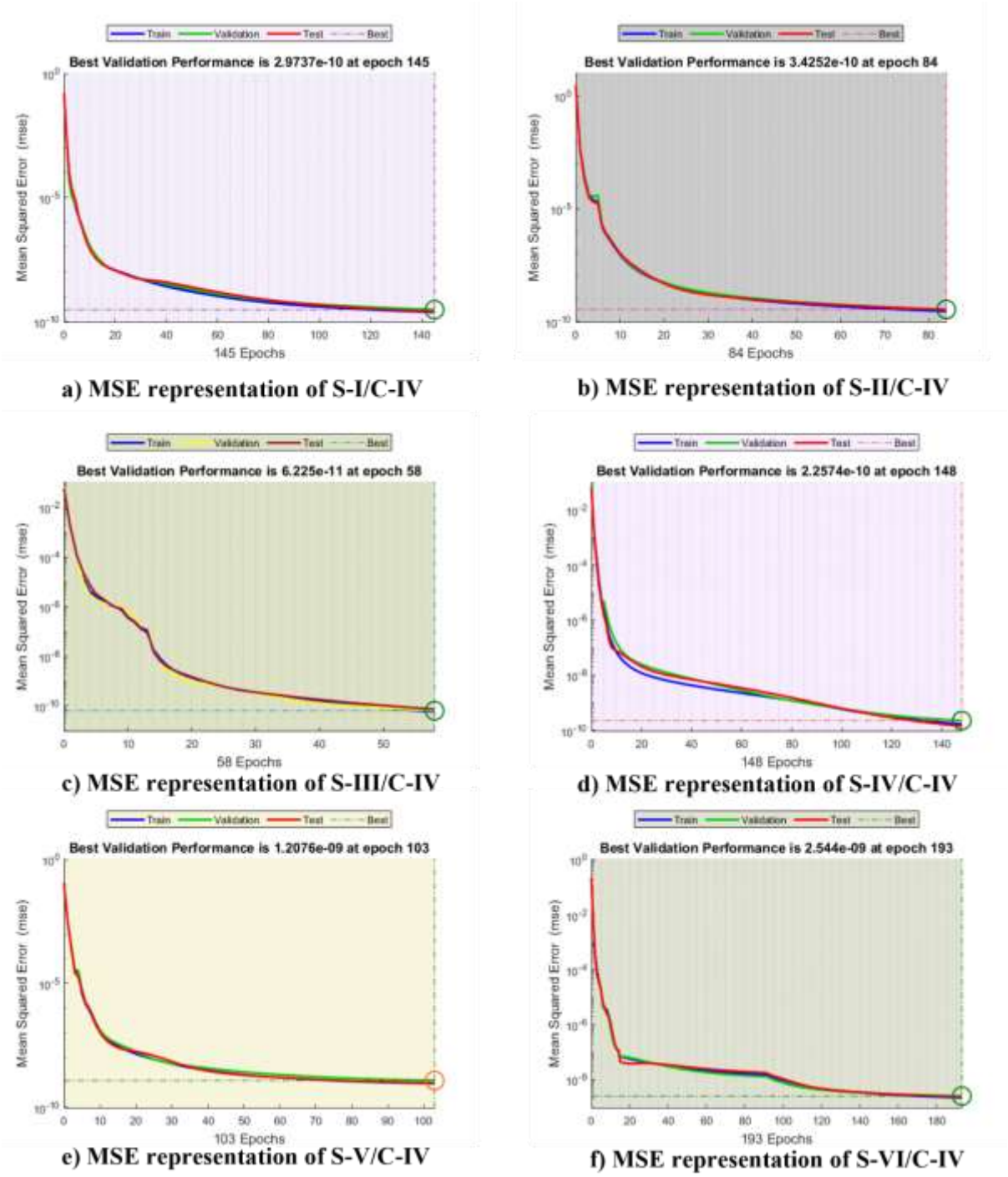

Figure 4. MSE representations of Case IV for all scenarios of the LBM-BN VSN.

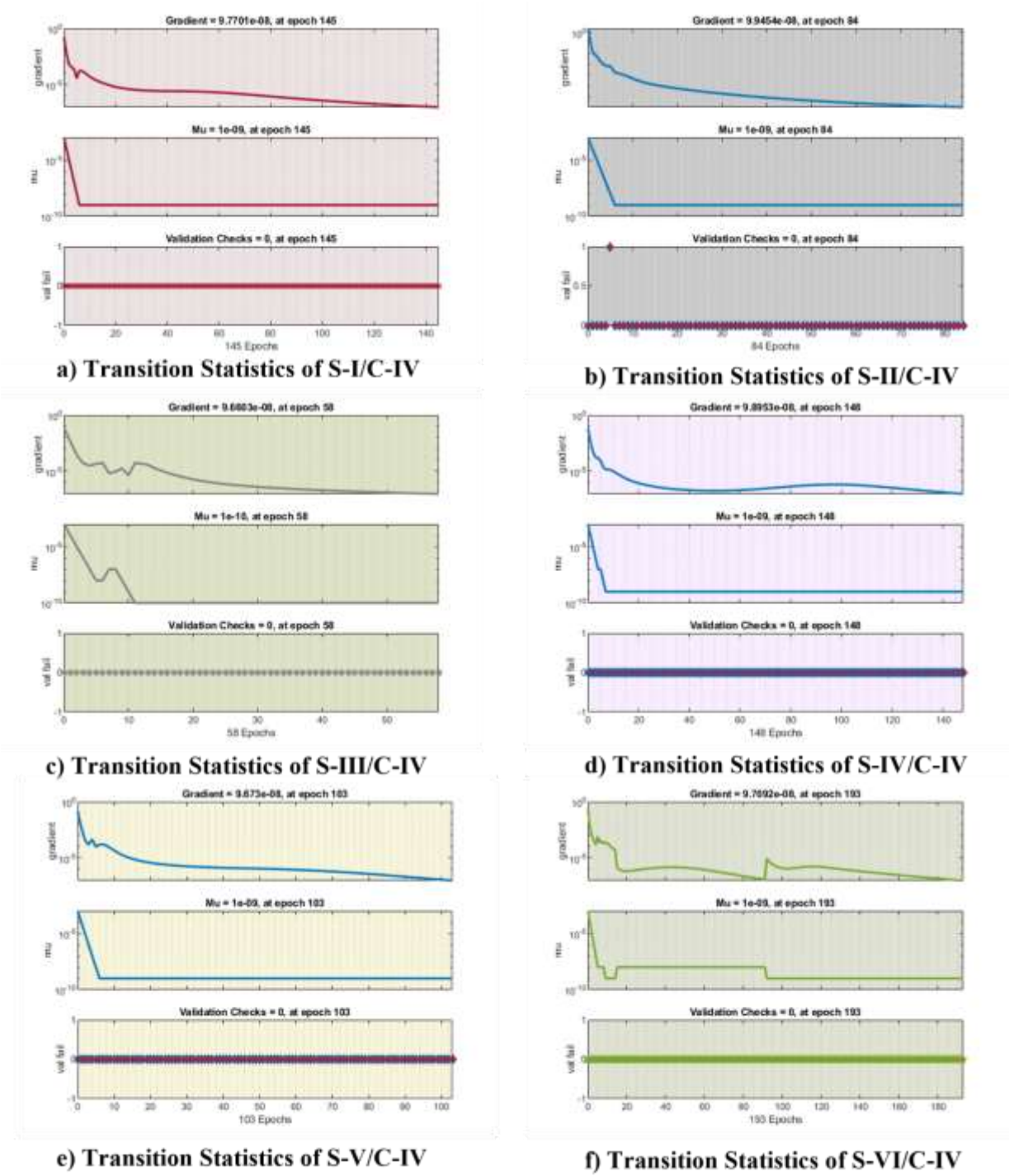

Figure 5. Graphical illustration of transition statistics for Case IV for all scenarios of the LBM-BN VSN.

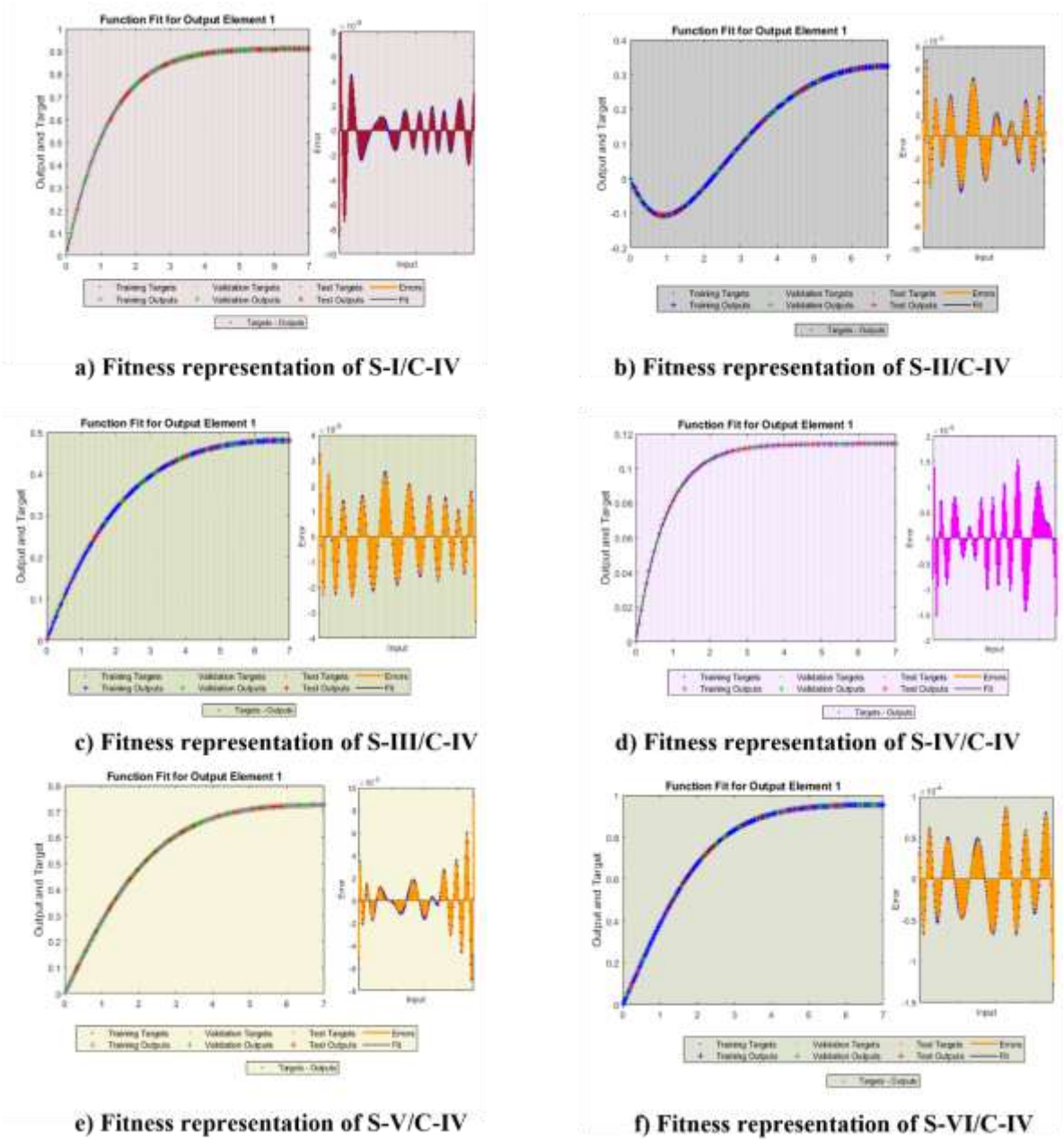

Figure 6. Graphical illustration of fitness representation of Case IV for all scenarios of the LBM-BN VSN.

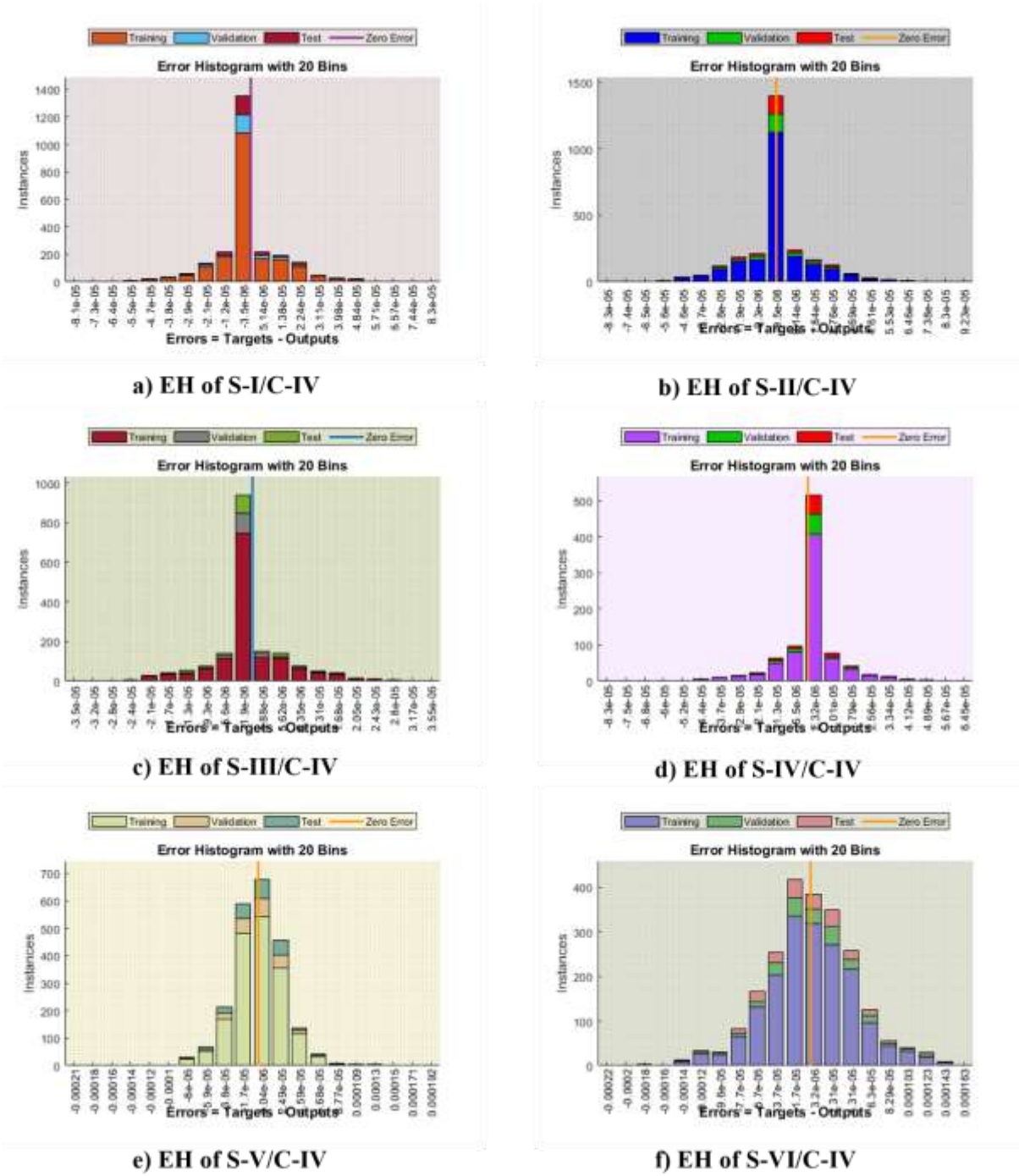

Figure 7. Graphical illustration of EH results for Case IV for all scenarios of the LBM-BN VSN.

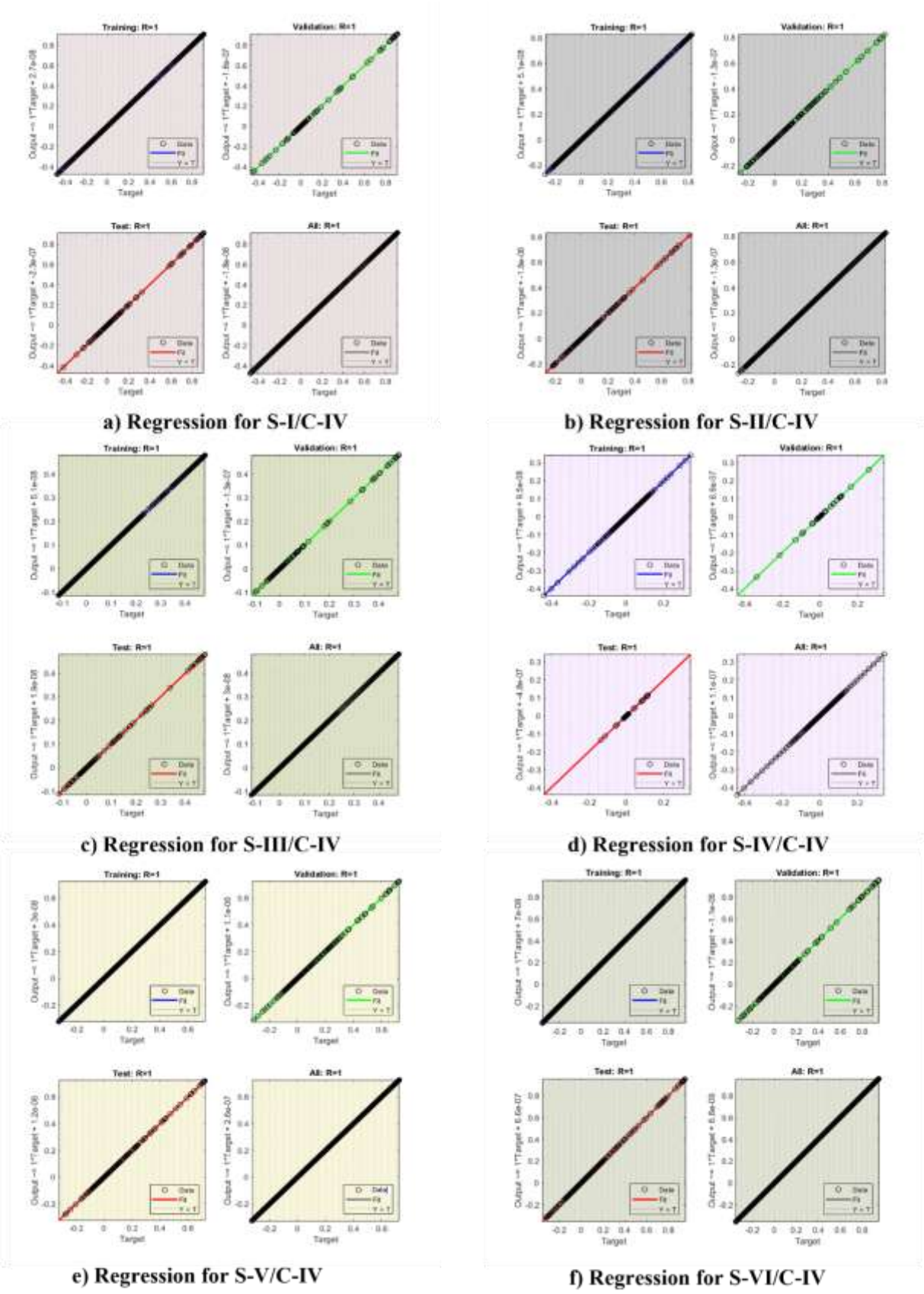

Figure 8. Graphical illustration of regression analysis results for Case IV for all scenarios of the LBM-BN VSN.

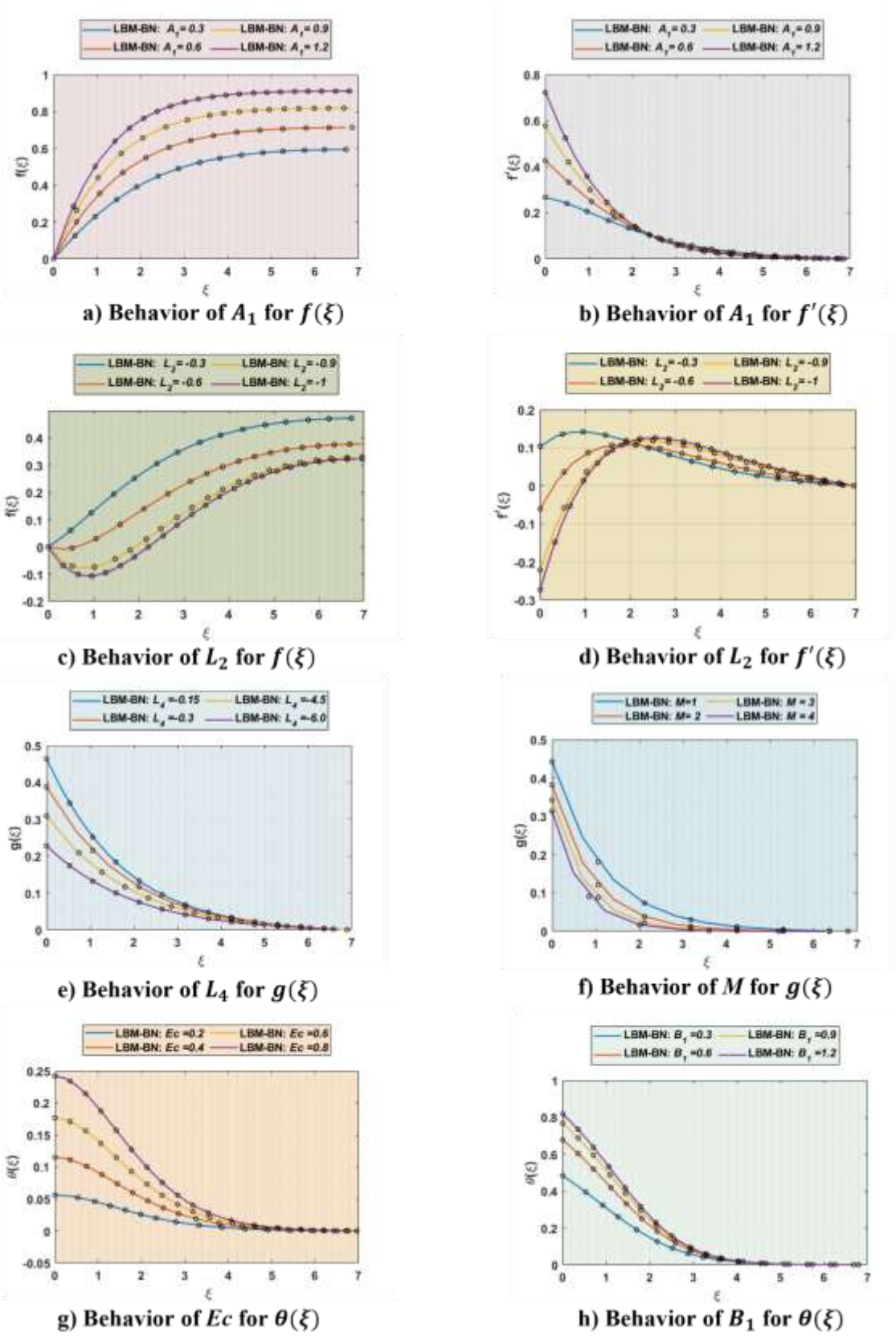

Figure 9. Comparison of numerical reference solutions with those of the LBM-BN according to variation of the influential parameters for $f(\xi)$, $f'(\xi)$, $g(\xi)$ and $\theta(\xi)$.

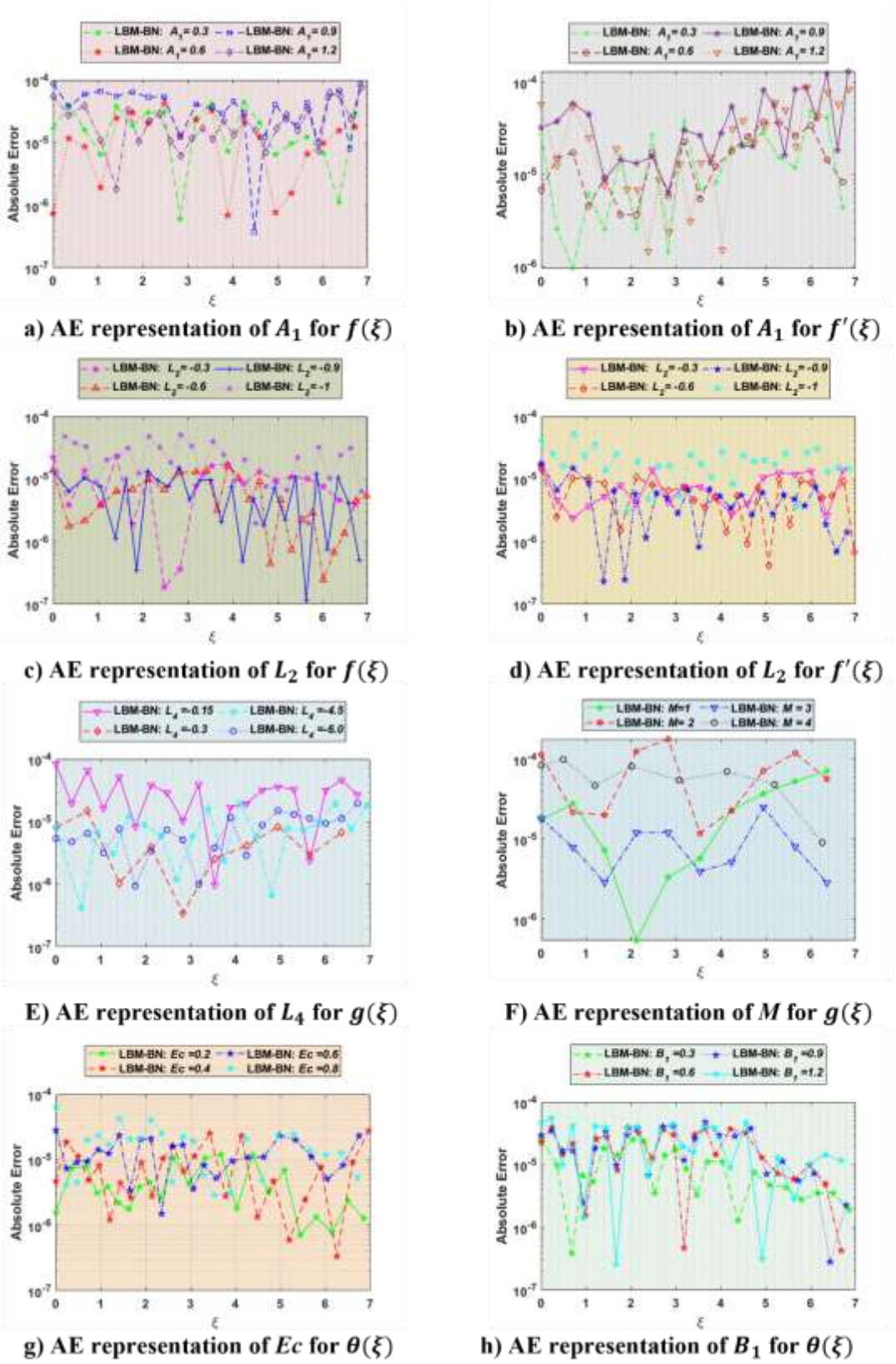

Figure 10. AE representation for the LBM-BN according to variation of the influential parameters for $f(\xi)$, $f'(\xi)$, $g(\xi)$ and $\theta(\xi)$.

5. Conclusions

For the present analysis, the author's main aim was exploitation of the concept of the VSN through the application of an LBM-BN to a stretched rotating disk for the inspection of a second-order velocity slip in the presence of activation energy. The PDEs indicating the VSN were converted into ODEs. The designed approach is efficient and accurate based on the MSEs obtained via the training, testing and validation procedures. Moreover, the convergence and stability of LBM-BN mappings have been validated on the basis of achieved accuracy through the application of regression-based statistical analysis and EHs for the proposed model. Lobatto IIIA was utilized to resolve the ODEs and generate the reference dataset for the LBM-BN. The reference dataset was used to facilitate calculation of the approximated solution of the VSN in MATLAB. The flow consequences on the $f(\xi), f'(\xi), g(\xi), \wedge \theta(\xi)$ profiles were analyzed from the perspectives of different physical quantities, i.e., A_1, M, L_2, L_4, B_1 and Ec. The substantial findings taken from this research are as follows:

- The axial and radial velocity functions grow as values of A_1 increase, but a reverse trend can be seen for L_2.
- The tangential velocity decreases with increment in L_4.
- With larger values of M, the tangential velocity increases.
- The temperature function is increased with increment in Ec and B_1.

Further, the proposed technique can also be applied to a micropolar nanofluid [54], a Casson nanofluid [55], the waterborne spread and control of diseases [56] and computer epidemic viruses [57]. As a future work direction, the authors will consider other machine learning techniques to study the activation energy of various chemical processes.

Acknowledgments

The authors extend their appreciation to the Deputyship for Research & Innovation, Ministry of Education in Saudi Arabia for funding this research work through the project number (IF2/PSAU/2022/01/21873).

Conflict of interest

The authors disclosed no conflicts of interest in publishing this paper.

References

1. H. B. Ly, M. H. Nguyen, B. T. Pham, Metaheuristic optimization of Levenberg-Marquardt-based artificial neural network using particle swarm optimization for prediction of foamed concrete compressive strength, *Neural Comput. Appl.*, **33** (2021), 17331–17351, https://doi.org/10.1007/s00521-021-06321-y
2. J. Zhao, H. Nguyen, T. Nguyen-Thoi, P. G. Asteris, J. Zhou, Improved Levenberg-Marquardt backpropagation neural network by particle swarm and whale optimization algorithms to predict the deflection of RC beams, *Eng. Comput.*, **38** (2022), 3847–3869, https://doi.org/10.1007/s00366-020-01267-6
3. H. X. Nguyen, H. Q. Cao, T. T. Nguyen, T. N. C. Tran, H. N. Tran, J. W. Jeon, Improving robot precision positioning using a neural network based on Levenberg Marquardt–APSO algorithm, *IEEE Access*, **9** (2021), 75415–75425, https://doi.org/10.1109/ACCESS.2021.3082534

4. M. S. Ali, M. Ayaz, T. Mansoor, Prediction of discharge through a sharp-crested triangular weir using ANN model trained with Levenberg-Marquardt algorithm, *Model. Earth Syst. Environ.*, **8** (2022), 1405–1417. https://doi.org/10.1007/s40808-021-01167-8
5. Z. Ye, M. K. Kim, Predicting electricity consumption in a building using an optimized backpropagation and Levenberg-Marquardt back-propagation neural network: case study of a shopping mall in China, *Sustain. Cities Soc.*, **42** (2018), 176–183, https://doi.org/10.1016/j.scs.2018.05.050
6. S. Bharati, M. A. Rahman, P. Podder, M. R. A. Robel, N. Gandhi, Comparative performance analysis of neural network base training algorithm and neuro-fuzzy system with SOM for the purpose of prediction of the features of superconductors, In: *International conference on intelligent systems design and applications*, Vol. 1181, Advances in Intelligent Systems and Computing, Springer, Cham, 2019, 69–79. https://doi.org/10.1007/978-3-030-49342-4_7
7. S. U. Choi, J. A. Eastman, *Enhancing thermal conductivity of fluids with nanoparticles*, 1995.
8. M. J. Uddin, O. A. Bég, A. I. Ismail, Radiative convective nanofluid flow past a stretching/shrinking sheet with slip effects, *J. Thermophys. Heat Transfer*, **29** (2015), 513–523. https://doi.org/10.2514/1.T4372
9. Z. U. Din, A. Ali, Z. A. Khan, G. Zaman, Heat transfer analysis: convective-radiative moving exponential porous fins with internal heat generation, *Math. Biosci. Eng.*, **19** (2022), 11491–11511. https://doi.org/10.3934/mbe.2022535
10. B. Jalili, S. Sadighi, P. Jalili, D. D. Ganji, Numerical analysis of MHD nanofluid flow and heat transfer in a circular porous medium containing a Cassini oval under the influence of the Lorentz and buoyancy forces, *Heat Transfer*, **51** (2022), 6122–6138. https://doi.org/10.1002/htj.22582
11. B. Jalili, P. Jalili, S. Sadighi, D. D. Ganji, Effect of magnetic and boundary parameters on flow characteristics analysis of micropolar ferrofluid through the shrinking sheet with effective thermal conductivity, *Chin. J. Phys.*, **71** (2021), 136–150. https://doi.org/10.1016/j.cjph.2020.02.034
12. B. P. Geridonmez, RBF simulation of natural convection in a nanofluid-filled cavity, *AIMS Math.*, **1** (2016), 195–207. https://doi.org/10.3934/Math.2016.3.195
13. M. Sheikholeslami, D. D. Ganji, H. R. Ashorynejad, Investigation of squeezing unsteady nanofluid flow using ADM, *Powder Technol.*, **239** (2013), 259–265. https://doi.org/10.1016/j.powtec.2013.02.006
14. A. Raza, M. Y. Almusawa, Q. Ali, A. U. Haq, K. Al-Khaled, I. E. Sarris, Solution of water and sodium alginate-based Casson type hybrid nanofluid with slip and sinusoidal heat conditions: a prabhakar fractional derivative approach, *Symmetry*, **14** (2022), 2658. https://doi.org/10.3390/sym14122658
15. J. V. Tawade, C. N. Guled, S. Noeiaghdam, U. Fernandez-Gamiz, V. Govindan, S. Balamuralitharan, Effects of thermophoresis and Brownian motion for thermal and chemically reacting Casson nanofluid flow over a linearly stretching sheet, *Results Eng.*, **15** (2022), 100448. https://doi.org/10.1016/j.rineng.2022.100448
16. M. Hamid, T. Zubair, M. Usman, R. U. Haq, Numerical investigation of fractional-order unsteady natural convective radiating flow of nanofluid in a vertical channel, *AIMS Math.*, **4** (2019), 1416–1429. https://doi.org/10.3934/math.2019.5.1416
17. S. Arulmozhi, K. Sukkiramathi, S. S. Santra, R. Edwan, U. Fernandez-Gamiz, S. Noeiaghdam, Heat and mass transfer analysis of radiative and chemical reactive effects on MHD nanofluid over an infinite moving vertical plate, *Results Eng.*, **14** (2022), 100394. https://doi.org/10.1016/j.rineng.2022.100394

18. M. S. Khan, S. Mei, Shabnam, U. Fernandez-Gamiz, S. Noeiaghdam, A. Khan, et al., Electroviscous effect of water-base nanofluid flow between two parallel disks with suction/injection effect, *Mathematics*, **10** (2022), 956. https://doi.org/10.3390/math10060956
19. F. Tuz Zohra, M. J. Uddin, M. F. Basir, A. I. M. Ismail, Magnetohydrodynamic bio-nano-convective slip flow with Stefan blowing effects over a rotating disc, *Proceedings of the Institution of Mechanical Engineers, Part N: Journal of Nanomaterials, Nanoengineering and Nanosystems*, **234** (2020), 83–97. https://doi.org/10.1177/2397791419881580
20. M. J. Uddin, N. A. Amirsom, O. A. Bég, A. I. Ismail, Computation of bio-nano-convection power law slip flow from a needle with blowing effects in a porous medium, *Waves Random Complex Media*, 2022, 1–21. https://doi.org/10.1080/17455030.2022.2048919
21. O. A. Bég, T. Bég, W. A. Khan, M. J. Uddin, Multiple slip effects on nanofluid dissipative flow in a converging/diverging channel: a numerical study, *Heat Transfer*, **51** (2022), 1040–1061. https://doi.org/10.1002/htj.22341
22. M. J. Uddin, W. A. Khan, A. I. Ismail, Lie group analysis and numerical solutions for magnetoconvective slip flow along a moving chemically reacting radiating plate in porous media with variable mass diffusivity, *Heat Transfer*, **45** (2016), 239–263, https://doi.org/10.1002/htj.21161
23. N. A. Amirsom, M. J. Uddin, M. F. M. Basir, A. I. M. Ismail, O. A. Bég, A. Kadir, Three-dimensional bioconvection nanofluid flow from a bi-axial stretching sheet with anisotropic slip, *Sains Malays.*, **48** (2019), 1137–1149, http://dx.doi.org/10.17576/jsm-2019-4805-23
24. M. Irfan, K. Rafiq, M. Khan, M. Waqas, M. S. Anwar, Theoretical analysis of new mass flux theory and Arrhenius activation energy in Carreau nanofluid with magnetic influence, *Int. Commun. Heat Mass Transfer*, **120** (2021), 105051. https://doi.org/10.1016/j.icheatmasstransfer.2020.105051
25. H. Waqas, A. Kafait, T. Muhammad, U. Farooq, Numerical study for bio-convection flow of tangent hyperbolic nanofluid over a Riga plate with activation energy, *Alex. Eng. J.*, **61** (2022), 1803–1814. https://doi.org/10.1016/j.aej.2021.06.068
26. M. M. Bhatti, E. E. Michaelides, Study of Arrhenius activation energy on the thermo-bioconvection nanofluid flow over a Riga plate, *J. Therm. Anal. Calorim.*, **143** (2021), 2029–2038. https://doi.org/10.1007/s10973-020-09492-3
27. T. Muhammad, H. Waqas, S. A. Khan, R. Ellahi, S. M. Sait, Significance of nonlinear thermal radiation in 3D Eyring–Powell nanofluid flow with Arrhenius activation energy, *J. Therm. Anal. Calorim.*, **143** (2021), 929–944. https://doi.org/10.1007/s10973-020-09459-4
28. D. Habib, N. Salamat, S. Abdal, I. Siddique, M. C. Ang, A. Ahmadian, On the role of bioconvection and activation energy for time dependent nanofluid slip transpiration due to extending domain in the presence of electric and magnetic fields, *Ain Shams Eng. J.*, **13** (2022), 101519. https://doi.org/10.1016/j.asej.2021.06.005
29. T. Hayat, Z. Nisar, A. Alsaedi, B. Ahmad, Analysis of activation energy and entropy generation in mixed convective peristaltic transport of Sutterby nanofluid, *J. Therm. Anal. Calorim.*, **143** (2021), 1867–1880. https://doi.org/10.1007/s10973-020-09969-1
30. M. Shoaib, G. Zubair, K. S. Nisar, M. A. Z. Raja, M. I. Khan, R. P. Gowda, et al., Ohmic heating effects and entropy generation for nanofluidic system of Ree-Eyring fluid: intelligent computing paradigm, *Int. Commun. Heat Mass Transfer*, **129** (2021), 105683. https://doi.org/10.1016/j.icheatmasstransfer.2021.105683

31. I. Ahmad, H. Ilyas, M. A. Z. Raja, Z. Khan, M. Shoaib, Stochastic numerical computing with Levenberg-Marquardt backpropagation for performance analysis of heat Sink of functionally graded material of the porous fin, *Surf. Interfaces*, **26** (2021), 101403. https://doi.org/10.1016/j.surfin.2021.101403
32. M. Shoaib, M. A. Z. Raja, M. T. Sabir, A. H. Bukhari, H. Alrabaiah, Z. Shah, et al., A stochastic numerical analysis based on hybrid NAR-RBFs networks nonlinear SITR model for novel COVID-19 dynamics, *Comput. Methods Programs Biomed.*, **202** (2021), 105973. https://doi.org/10.1016/j.cmpb.2021.105973
33. A. Shafiq, A. B. Çolak, T. N. Sindhu, Q. M. Al-Mdallal, T. Abdeljawad, Estimation of unsteady hydromagnetic Williamson fluid flow in a radiative surface through numerical and artificial neural network modeling, *Sci. Rep.*, **11** (2021), 1–21. https://doi.org/10.1038/s41598-021-93790-9
34. A. Shafiq, A. B. Çolak, T. Naz Sindhu, Designing artificial neural network of nanoparticle diameter and solid–fluid interfacial layer on single walled carbon nanotubes/ethylene glycol nanofluid flow on thin slendering needles, *Int. J. Numer. Methods Fluids*, **93** (2021), 3384–3404. https://doi.org/10.1002/fld.5038
35. Z. Sabir, M. A. Z. Raja, J. L. Guirao, M. Shoaib, Integrated intelligent computing with neuro-swarming solver for multi-singular fourth-order nonlinear Emden–Fowler equation, *Comput. Appl. Math.*, **39** (2020), 1–18. https://doi.org/10.1007/s40314-020-01330-4
36. Z. Sabir, M. A. Z. Raja, M. Umar, M. Shoaib, Neuro-swarm intelligent computing to solve the second-order singular functional differential model, *Eur. Phys. J. Plus*, **135** (2020), 474. https://doi.org/10.1140/epjp/s13360-020-00440-6
37. A. Shafiq, A. B. Çolak, T. N. Sindhu, T. Muhammad, Optimization of Darcy-Forchheimer squeezing flow in nonlinear stratified fluid under convective conditions with artificial neural network, *Heat Transfer Res.*, **53** (2022), 67–89. https://doi.org/10.1615/HeatTransRes.2021041018
38. M. Shoaib, M. Kausar, K. S. Nisar, M. A. Z. Raja, M. Zeb, A. Morsy, The design of intelligent networks for entropy generation in Ree-Eyring dissipative fluid flow system along quartic autocatalysis chemical reactions, *Int. Commun. Heat Mass Transfer*, **133** (2022), 105971. http://doi.org/10.1016/j.icheatmasstransfer.2022.105971
39. M. Umar, M. A. Z. Raja, Z. Sabir, A. S. Alwabli, M. Shoaib, A stochastic computational intelligent solver for numerical treatment of mosquito dispersal model in a heterogeneous environment, *Eur. Phys. J. Plus*, **135** (2020), 1–23. https://doi.org/10.1140/epjp/s13360-020-00557-8
40. M. Umar, Kusen, M. A. Z. Raja, Z. Sabir, Q. Al-Mdallal, A computational framework to solve the nonlinear dengue fever SIR system, *Comput. Methods Biomech. Biomed. Eng.*, **25** (2022), 1821–1834. https://doi.org/10.1080/10255842.2022.2039640
41. Z. Sabir, S. Ben Said, Q. Al-Mdallal, A fractional order numerical study for the influenza disease mathematical model, *Alex. Eng. J.*, 2022. https://doi.org/10.1016/j.aej.2022.09.034
42. T. Botmart, Z. Sabir, A. S. Alwabli, S. B. Said, Q. Al-Mdallal, M. E. Camargo, et al., Computational stochastic investigations for the socio-ecological dynamics with reef ecosystems, *Comput. Mater. Continua*, **73** (2022), 5589–5607. https://doi.org/10.32604/cmc.2022.032087
43. M. Umar, F. Amin, Q. Al-Mdallal, M. R. Ali, A stochastic computing procedure to solve the dynamics of prevention in HIV system, *Biomed. Signal Process. Control*, **78** (2022), 103888. https://doi.org/10.1016/j.bspc.2022.103888

44. S. Z. Abbas, M. I. Khan, S. Kadry, W. A. Khan, M. Israr-Ur-Rehman, M. Waqas, Fully developed entropy optimized second order velocity slip MHD nanofluid flow with activation energy, *Comput. Meth. Prog. Biomed.*, **190** (2020), 105362. https://doi.org/10.1016/j.cmpb.2020.105362
45. S. Qayyum, T. Hayat, M. I. Khan, M. I. Khan, A. Alsaedi, Optimization of entropy generation and dissipative nonlinear radiative Von Karman's swirling flow with Soret and Dufour effects, *J. Mol. Liq.*, **262** (2018), 261–274, https://doi.org/10.1016/j.molliq.2018.04.010
46. S. Qayyum, M. I. Khan, T. Hayat, A. Alsaedi, M. Tamoor, Entropy generation in dissipative flow of Williamson fluid between two rotating disks, *Int. J. Heat Mass Transfer*, **127** (2018), 933–942. https://doi.org/10.1016/j.ijheatmasstransfer.2018.08.034
47. M. Turkyilmazoglu, MHD fluid flow and heat transfer due to a shrinking rotating disk, *Comput. Fluids*, **90** (2014), 51–56. https://doi.org/10.1016/j.compfluid.2013.11.005
48. M. Shoaib, M. A. Z. Raja, M. T. Sabir, M. Awais, S. Islam, Z. Shah, et al., Numerical analysis of 3-D MHD hybrid nanofluid over a rotational disk in presence of thermal radiation with Joule heating and viscous dissipation effects using Lobatto IIIA technique, *Alex. Eng. J.*, **60** (2021), 3605–3619. https://doi.org/10.1016/j.aej.2021.02.015
49. C. Ouyang, R. Akhtar, M. A. Z. Raja, M. Touseef Sabir, M. Awais, M. Shoaib, Numerical treatment with Lobatto IIIA technique for radiative flow of MHD hybrid nanofluid (Al_2O_3—Cu/H_2O) over a convectively heated stretchable rotating disk with velocity slip effects, *AIP Adv.*, **10** (2020), 055122. https://doi.org/10.1063/1.5143937
50. M. Shoaib, M. A. Z. Raja, M. T. Sabir, S. Islam, Z. Shah, P. Kumam, et al., Numerical investigation for rotating flow of MHD hybrid nanofluid with thermal radiation over a stretching sheet, *Sci. Rep.*, **10** (2020), 1–15. https://doi.org/10.1038/s41598-020-75254-8
51. B. V. Rogov, Dispersive and dissipative properties of the fully discrete bicompact schemes of the fourth order of spatial approximation for hyperbolic equations, *Appl. Numer. Math.*, **139** (2019), 136–155, https://doi.org/10.1016/j.apnum.2019.01.008
52. M. Shoaib, M. Kausar, M. I. Khan, M. Zeb, R. P. Gowda, B. C. Prasannakumara, et al., Intelligent backpropagated neural networks application on Darcy-Forchheimer ferrofluid slip flow system, *Int. Commun. Heat Mass Transfer*, **129** (2021), 105730. https://doi.org/10.1016/j.icheatmasstransfer.2021.105730
53. M. Shoaib, M. A. Z. Raja, M. A. R. Khan, I. Farhat, S. E. Awan, Neuro-computing networks for entropy generation under the influence of MHD and thermal radiation, *Surf. Interfaces*, **25** (2021), 101243. https://doi.org/10.1016/j.surfin.2021.101243
54. S. E. Awan, M. A. Z. Raja, F. Gul, Z. A. Khan, A. Mehmood, M. Shoaib, Numerical computing paradigm for investigation of micropolar nanofluid flow between parallel plates system with impact of electrical MHD and hall current, *Arab. J. Sci. Eng.*, **46** (2021), 645–662. https://doi.org/10.1007/s13369-020-04736-8
55. M. Shoaib, M. A. Z. Raja, W. Jamshed, K. S. Nisar, I. Khan, I. Farhat, Intelligent computing Levenberg Marquardt approach for entropy optimized single-phase comparative study of second grade nanofluidic system, *Int. Commun. Heat Mass Transfer*, **127** (2021), 105544. https://doi.org/10.1016/j.icheatmasstransfer.2021.105544
56. N. Ruttanaprommarin, Z. Sabir, R. A. S. Núñez, S. Salahshour, J. L. G. Guirao, W. Weera, et al., Artificial neural network procedures for the waterborne spread and control of diseases, *AIMS Math.*, **8** (2023), 2435–2452. https://doi.org/10.3934/math.2023126
57. W. Weera, T. Botmart, T. La-inchua, Z. Sabir, R. A. S. Núñez, M. Abukhaled, et al., A stochastic computational scheme for the computer epidemic virus with delay effects, *AIMS Math.*, **8** (2023), 148–163. https://doi.org/10.3934/math.2023007

Appendix

Nomenclature:

NN	Neural network	ANN	Artificial neural network
NF	Nanofluid	$AE\,(J)$	Activation energy
$T\,(K)$	Temperature	u, v, w	Velocity component
C	Concentration	r, v, z	Coordinates system
T_∞	Ambient temperature	$\sigma_f\,(S/m)$	Electrical conductivity
C_∞	Ambient concentration	$\rho_f\,(kg/m^3)$	Density
$g\,(m/s^2)$	Gravitational acceleration	$B_0\,(Tesla)$	Strength of magnetic field
a_1	Dimensional or stretching constant	N	Ratio of concentration to temperature buoyancy force
D_T	Thermophoretic diffusion	σ	Stefan-Boltzman constant
κ_r	Chemical reaction rate	κ	Mean absorption coefficient
D_B	Brownian diffusion	n	Fitted rate constant
E_a	Coefficient of activation energy	Ω	Angular frequency
$\kappa_f\,(Wm^{-1}K^{-1})$	Thermal conductivity	T_w	Fluid temperature
h_1	Heat transfer coefficients	h_2	Mass transfer coefficients
κ	Boltzmann constant	$C_w\,(M)$	Fluid concentration
$\Re$	Reynolds number	M	Magnetic variable
λ	Mixed convection variable	C_p	Specific heat
Pr	Prandtl number	R	Radiation parameter
Nt	Thermophoretic parameter	Ec	Eckert number
Nb	Brownian motion parameter	Sc	Schmidt number
κ_1	Chemical reaction parameter	α_1	Temperature ratio parameter
β_t	Nonlinear convection parameters related to temperature	$\beta_c\,(M)$	Nonlinear convection parameters related to concentration
E_1	Activation energy parameter	A_1	Stretching parameter
L_1, L_3	First-order slip parameters	L_2, L_4	Second-order slip parameters
B_1	Thermal Biot numbers	B_2	Solutal Biot numbers
LM	Levenberg-Marquardt	MHD	Magnetohydrodynamic
λ_1, λ_3	First-order slip coefficient for velocity	λ_2, λ_4	Second-order slip coefficient for velocity
MSE	Mean square error	TS	Transition state
MHD	Magnetohydrodynamics	AE	Absolute error
EH	Error histogram	VSN	Second-order velocity slip nanofluid
$LBM-BN$	Levenberg-Marquardt backpropagation artificial neural network	AI	Artificial intelligence